

A comparison of full vs. fast simulation observables describing jets at CLD

Sara Aumiller, Michele Selvaggi, Dolores Garcia

July 24, 2024

We describe detectors with fast simulation or full simulation. Using particle flow objects we can extract observables characterizing jets and their constituents from both types of simulation. The observables are used as input parameters for a neural network which performs jet flavor tagging which is for example important for Higgs physics. We provide a comparison of the observables extracted from fast simulation and full simulation of the proposed CLD detector at FCC-ee.

Contents

1	The collection of parameters	1
1.1	Fast Simulation Parameters	1
1.2	Full Simulation Parameters	3
1.3	Suggestions for improvement	4
2	Comparing fast vs. full simulation distributions	4
2.1	Jet description	4
2.2	Jet constituents	4
2.2.1	Charged jet constituents	5
2.2.2	Neutral jet constituents	6
3	Comparing H to $q\bar{q}$ processes in full simulation	6
3.1	Jet constituents	6
3.1.1	Charged jet constituents	7
3.1.2	Neutral jet constituents	7
3.1.3	Explanation of the peaks in <code>pfcand_phirel</code>	8
4	Mathematical derivation of $\frac{\pi}{2}$ peaks	9
5	Conclusion	11

1 The collection of parameters

1.1 Fast Simulation Parameters

An overview of the parameters in fast simulation is given below:

Jet flavor

The jet flavor is extracted from the file name and not from the reconstruction:

- `recojet_isG`: jet originates from gluon
- `recojet_isU`: jet originates from u or \bar{u} quark
- `recojet_isD`: jet originates from d or \bar{d} quark
- `recojet_isS`: jet originates from s or \bar{s} quark
- `recojet_isC`: jet originates from c or \bar{c} quark
- `recojet_isB`: jet originates from b or \bar{b} quark
- `recojet_isTAU`: jet originates from τ or $\bar{\tau}$ lepton

Jet description

- `jet_p`: magnitude of three-momentum
- `jet_e`: energy
- `jet_mass`: mass
- `jet_phi`: azimuthal angle
- `jet_theta`: polar angle

We count the amount of particles in the jet:

- `jet_nconst = jet_npfcand`: number of constituents / particles / particle flow candidates in jet
- `jet_nmu`: number of muons
- `jet_nel`: number of electrons
- `jet_nchad`: number of charged hadrons
- `jet_ngamma`: number of photons
- `jet_nnhad`: number of neutral hadrons

Jet constituents

One jet is composed of several constituents. They can be described with:

- `pfcand_e`: energy of particle in jet
- `pfcand_p`: momentum of particle in jet
- `pfcand_theta`: polar angle of particle
- `pfcand_phi`: azimuthal angle of particle
- `pfcand_erelel_log`: $\log \frac{E}{E_{\text{jet}}}$ energy of the jet constituent divided by the jet energy
- `pfcand_thetarel`: θ_{rel} polar angle of the constituent with respect to the jet momentum
- `pfcand_phirel`: ϕ_{rel} azimuthal angle of the constituent with respect to the jet momentum

The following 15 parameters are describing the covariance matrix of the helix track:
`pfcand_dptdpt`, `pfcand_detadeta`, `pfcand_dphidphi`, `pfcand_dxydxy`, `pfcand_dzdz`, `pfcand_dxydz`,
`pfcand_dphidxy`, `pfcand_dlambdadz`, `pfcand_dxyc`, `pfcand_dxyctgtheta`, `pfcand_phic`, `pfcand_phidz`,
`pfcand_phictgtheta`, `pfcand_cdz`, `pfcand_cctgtheta`. These are the lower triangular entries of a 5x5 covariance matrix describing the helix track with the five parameter: d_0 (referred to as xy), ϕ , Ω (or p_t), z_0 , $\tan(\lambda)$.

Identification parameters:

- `pfcand_mt0f`: mass through time of flight
- `pfcand_dndx`: dN/dx similar to dE/dx for PID
- `pfcand_charge`: $\in -1, 0, 1$
- `pfcand_isMu`: boolean
- `pfcand_isEl`: boolean
- `pfcand_isChargedHad`: boolean
- `pfcand_isGamma`: boolean
- `pfcand_isNeutralHad`: boolean
- `pfcand_type`: reconstructed PDG particle ID (e.g. 22 = photon)

Parameters describing the displacement of the track:

- `pfcand_dxy`: displacement of vertex in dr direction = transverse impact parameter of the track
- `pfcand_dz`: displacement of vertex in dz (beam) direction = longitudinal impact parameter of the track
- `pfcand_btagSip2dVal`: SIP_{2D}: signed 2D impact parameter of the track
- `pfcand_btagSip2dSig`: SIP_{2D}/ σ_{2D} : signed 2D impact parameter significance of the track
- `pfcand_btagSip3dVal`: SIP_{3D}: signed 3D impact parameter of the track
- `pfcand_btagSip3dSig`: SIP_{3D}/ σ_{3D} : signed 3D impact parameter significance of the track
- `pfcand_btagJetDistVal`: d_{3D} : jet track distance at their point of closest approach
- `pfcand_btagJetDistSig`: $d_{3D}/\sigma_{d_{3D}}$: jet track distance significance at their point of closest approach

1.2 Full Simulation Parameters

We want to extract the same parameters as in fast simulation for full simulation. Here are some remarks on the differences occurring when using full simulation:

- `jet_nconst` and `jet_npf` are filled in the same way, they are the same parameter.
We keep them for completeness.
- `pfcand_mt0f` and `pfcand_dndx` are set to zero in full simulation because we have no TPC or equivalent detector at CLD yet.

- `pfcand_btagSip2dSig`, `pfcand_btagSip3dSig`, `pfcand_btagJetDistSig` values for neutral particles is -200 instead of -9 like in fast simulation so that the value sits outside the distribution.
- we added a new parameter called `pfcand_MCPID` which is the PDG particle ID of the particles in the jet. It is the true MC particle ID. This might be useful in the future to test the limits of the neural network.
- we will also extract information about secondary vertices and V^0 for better tagging performance.

1.3 Suggestions for improvement

When extracting the parameters, we found some processes that could be optimized. These are:

- When calculating the parameters with respect to the primary vertex instead of $(0, 0, 0)$, the changes in the covariance matrix are not considered.
- When calculating the parameters with respect to the primary vertex instead of $(0, 0, 0)$, the changes in the relative angles `pfcand_relphi`, `pfcand_reltheta` are not considered.

2 Comparing fast vs. full simulation distributions

To understand the differences between full and fast simulation we plot the distributions of the parameters. Exemplary, we choose an $H \rightarrow b\bar{b}$ process. The data consists of 15k jets for full and fast simulation at CLD. To compare them, we normalize the distributions so that "the result is the value of the probability density function at the bin, normalized such that the integral over the range is 1" [1]. The sum of the histogram values is therefore not necessarily 1. We use overflow bins at the edge of the histograms to count the number of events that fall outside the range of the histograms.

2.1 Jet description

Considering the jet description, we see in Figure 1 and Figure 2 that the distributions are similar. We notice the different conventions in ϕ which is $\phi \in [0, 2\pi]$ in fast simulation and $\phi \in [-\pi, \pi]$ in full simulation. We can see that the full simulation has more neutral hadrons per jet.

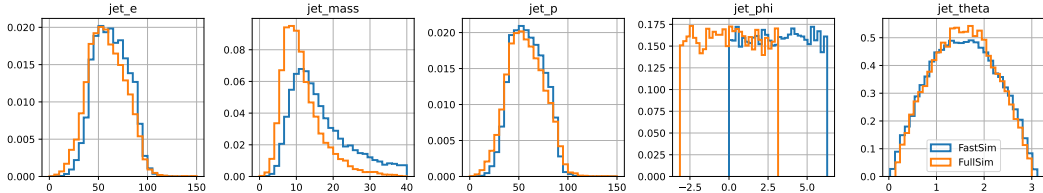


Figure 1: Jet properties in fast (blue) and full (orange) simulation

2.2 Jet constituents

To test the properties of the jet constituents we separate the particles in charged and neutral particles as the charged particles leave a track which we can describe in much detail. For

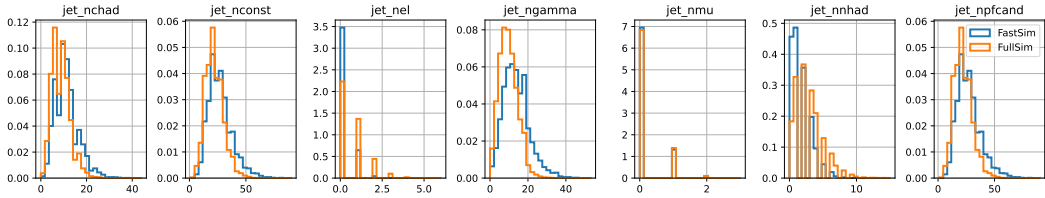


Figure 2: Jet multiplicities in fast (blue) and full (orange) simulation

neutral particles these values are always set to -9 (only in the case of `pfcand_btagSip2dSig`, `pfcand_btagSip3dSig`, `pfcand_btagJetDistSig` they are set to -200 to sit outside the distribution). We look at three leading charged/neutral particles to consider particles carrying the highest amount of energy in the jet.

2.2.1 Charged jet constituents

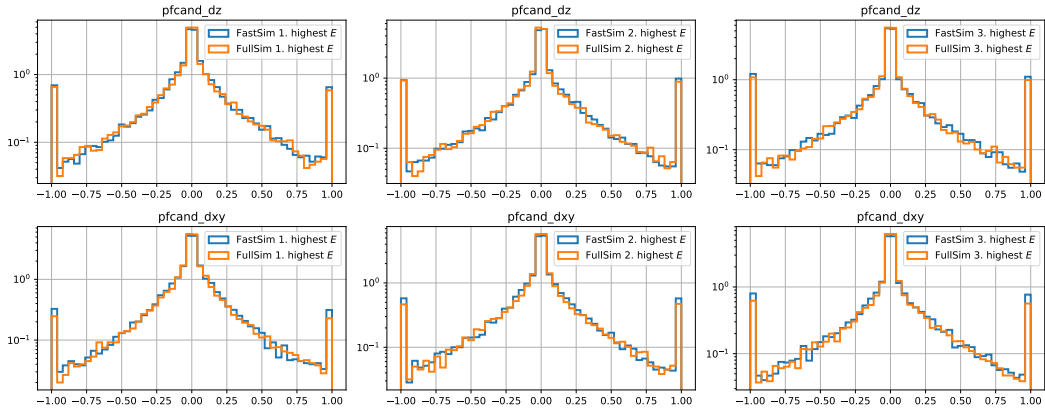


Figure 3: Impact parameters of the three leading (leading, subleading, third from left to right) charged particles in fast (blue) and full (orange) simulation in logarithmic scale

First, we look at charged particles in the jet. The histogram of the properties of the particles can be found in the Appendix, Figure 10. We see that the distributions are similar in the three leading particles. We observe the different tails in the `jet_reltheta` parameter: fast simulation has a longer tails than full simulation. For completeness, we show the same histograms in logarithmic scale in Figure 11 and verify that the histograms look similar even in logarithmic scale.

Next, we study the track properties. The impact parameters in fast and full simulation look similar even in logarithmic scale, see Figure 3, as well as the signed impact parameters (SIP) and distance of the particle track to the point of closest approach to the primary vertex and their regarding significances, see Figure 12. There is one issue one might consider investigating in the future. We would expect a dip in the 2D SIP significance as described in [2]. We can not observe this dip, neither in full nor in fast simulation for the 2D SIP values and significance, see Figure 4. We expect this dip at zero because we are calculating some kind of distance $r = \sqrt{x^2 + y^2}$ for gaussian distributions x and y which will give us a distribution close to zero at zero. Maybe resolution effects or the incorrect calculation of the covariance matrix are the reason for this. This should be investigated further. Such a dip can be observed for the 3D SIP significance in fast and full simulation which raises the question about the missing dip in the 2D SIP significance too.

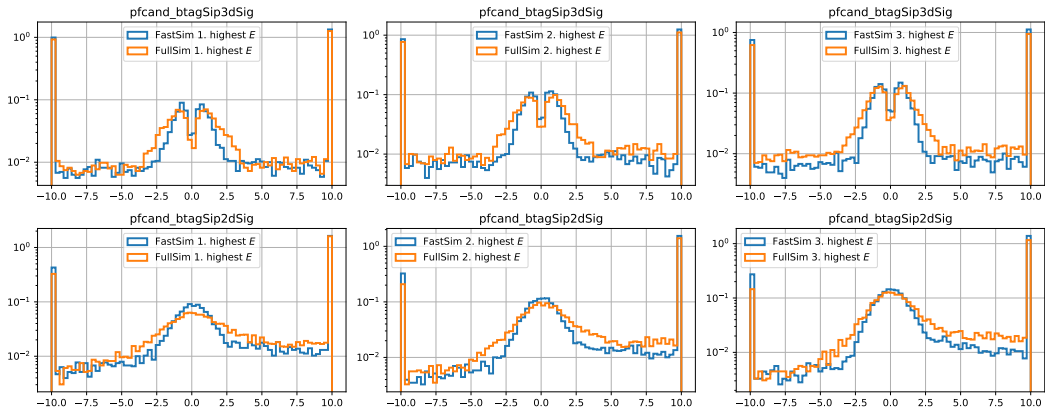


Figure 4: 2D and 3D SIP significances in fast vs. full simulation for H to $b\bar{b}$ process for the three leading (leading, subleading, third from left to right) particles (left to right descending energies). We can see a dip in the 3D SIP significance but not in the 2D SIP significance.

The histograms for the covariance matrix of the helix track are shown in Figure 13 and Figure 14 in the Appendix. Some distribution fit very well e.g. `pfcand_detadeta`, `pfcand_dlambdadz` or `pfcand_dphidphi` while others seem smeared out (`pfcand_phidz`, `pfcand_cctgtheta` or `pfcand_phictgtheta`). Two distributions do not match especially in higher orders: `pfcand_phic` and `pfcand_dxyc`.

2.2.2 Neutral jet constituents

We further separate the neutral particles into hadrons and leptons (photons). As these particles do not leave tracks, all the track related parameters are set to -9 (or -200). The histograms of their properties can be found in the Appendix (for hadrons, see Figure 15 and for photons, see Figure 16). Three observables show deviations between fast and full simulation: `pfcand_phirel` has peaks around $\pm \frac{\pi}{2}$ in full simulation (this will be discussed in Section 3.1.3) and `pfcand_thetarel` has longer tails in the case of neutral hadrons in fast simulation. `pfcand_theta` has peaks at π and 0 in fast simulation when looking at neutral hadrons and photons. This means these particles move along the beam axis. These photons might be initial state radiation. In FastSim, the calorimeter has an acceptance closer to the beam line than the tracking system, so charged hadrons coming as secondary particles from initial state radiation will all be reconstructed as neutrals. Full simulation is probably not able to reconstruct initial state radiation.

3 Comparing H to $q\bar{q}$ processes in full simulation

As we have observed similarity between H to $b\bar{b}$ processes in fast and full simulation, we want to confirm accordance for the other decay channels of the Higgs boson too. Therefore, we compare 15k H to $u\bar{u}$, H to $d\bar{d}$, H to $c\bar{c}$, H to $s\bar{s}$, H to $b\bar{b}$, H to $g\bar{g}$ and H to $\tau\bar{\tau}$ processes in full simulation. The jet properties and multiplicities can be seen in Figure 5 and Figure 6. We see accordance between the different quark channels. The τ channel looks different because the τ is a lepton and does not perform hadronisation. Therefore, it has less constituents and as a consequence also a smaller jet mass and lower energy/momentum.

3.1 Jet constituents

As before, we will analyze the jet constituents by separating them into charged and neutral particles. We look at the three leading particles of each category in the jet.

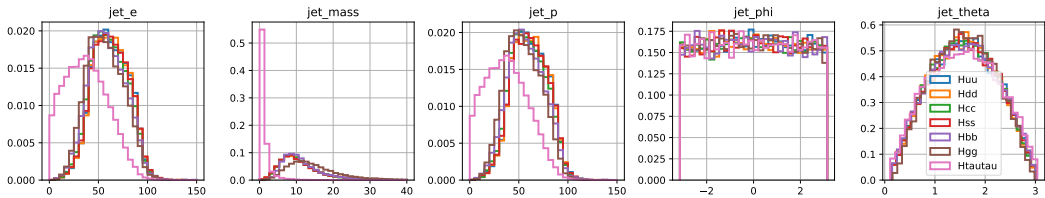


Figure 5: Jet properties in full simulation for $H \rightarrow q\bar{q}$ and $H \rightarrow \tau\bar{\tau}$ processes

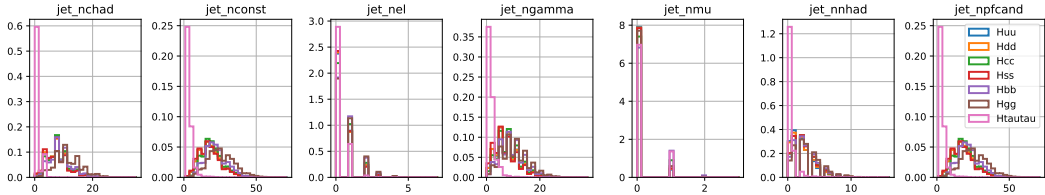


Figure 6: Jet multiplicities in full simulation for $H \rightarrow q\bar{q}$ and $H \rightarrow \tau\bar{\tau}$ processes

3.1.1 Charged jet constituents

Looking at the properties of the charged jet constituents in Figure 17 we can see accordance between the different Higgs decay channels. We observe that gluons and b quarks have higher energy compared to the other channels. The τ channel is again different from the quark channels. It has lower energies and smaller relative angles in θ . We see peaks in `pfcand_phirel` at $0 \pm \frac{\pi}{s}, \pi$ in the leading charged particle τ channel which we will explain in Section 3.1.3. Looking at the impact parameters in Figure 7 we observe the expected behavior of larger impact parameters for b and c quarks. Also the τ channel has larger impact parameters. The distributions are in accordance to our expectation. We can see similar behavior in the signed impact parameters and the distance to the point of closest approach in Figure 18. As expected, we can observe an asymmetry in the 2D SIP values and its significance. As b and c quarks will form short lived B (D) mesons, they travel a short distance before decaying in secondary vertices [2]. The vertices are always shifted into the direction of the jet momentum. This is why we observe the asymmetry around zero to the left and right in the 2D SIP values and significance. The covariance matrices of the helix track parameters can be seen in Figure 19 and Figure 20. All values show accordance between the different Higgs decay channels.

3.1.2 Neutral jet constituents

For completeness, we also show the properties of the three leading neutral hadrons and photons in the jet in the Appendix. The histograms describing the properties of the neutral constituents can be found in Figure 21 and Figure 22. The distributions seem mostly to match between the different Higgs decay channels. As previously seen comparing fast vs. full simulation, we see peaks around $\pm \frac{p_t}{2}$ for `pfcand_phirel` in all channels although one might expect a flat distribution. This will be discussed in Section 3.1.3. An other unexpected behavior are peaks at $\frac{\pi}{4}$ and $\frac{3\pi}{4}$ in `pfcand_theta` considering neutral hadrons. This is especially dominant in lower leading orders and for the τ channel. These angles correspond to the transition from the barrel to the end-caps in the detector. This might lead to wrong reconstruction, e.g. wrong/missing assignment of tracks to clusters which might lead to more reconstructed neutrals at these angles.

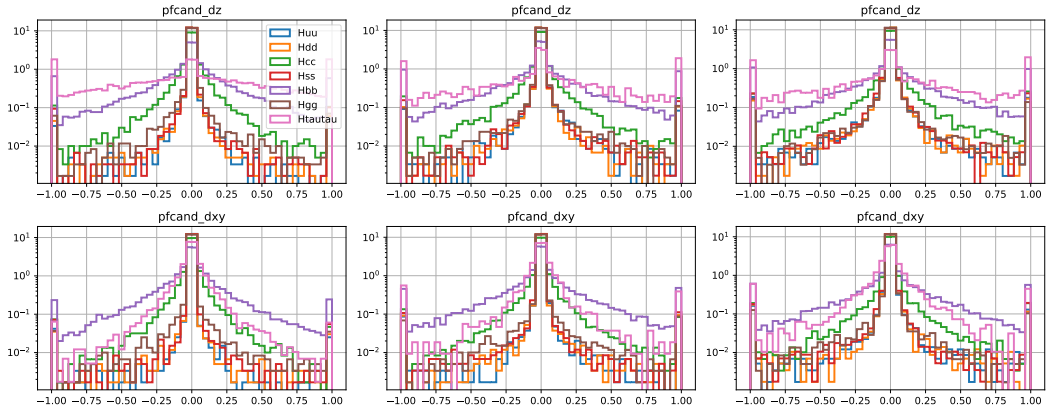


Figure 7: Impact parameters of the three leading (leading, subleading, third from left to right) charged particles in full simulation for $H \rightarrow q\bar{q}$ and $H \rightarrow \tau\bar{\tau}$ processes in logarithmic scale

3.1.3 Explanation of the peaks in pfcand_phirel

In this section, we want to explain the peaks at $\frac{\pi}{2}$ in the `pfcand_phirel` distribution observed in the τ channel for charged particles, see Figure 17, observed in all channels for neutral hadrons, see Figure 21 and also observed for photon constituent mainly for the τ channel, see Figure 22. We expect a flat distribution for $\Delta\phi$ because the polar angle should be arbitrary around the jet. As these peaks are very prominent in the τ channel, we start our investigation there.

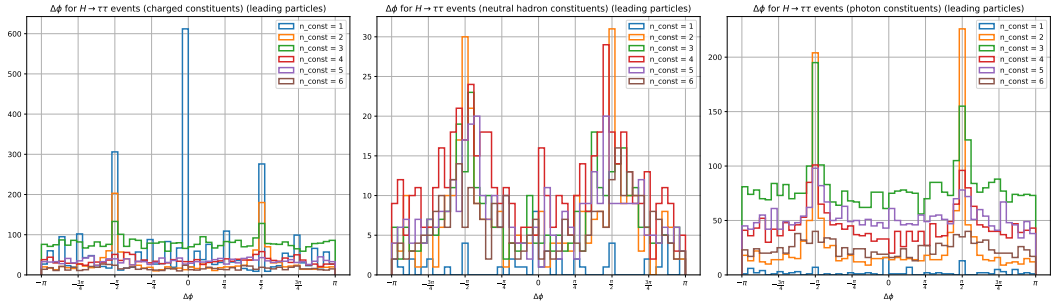


Figure 8: Separating the $\Delta\phi$ distribution by the number of constituents in the jet for $H \rightarrow \tau\bar{\tau}$ events. Charged constituents, neutral hadrons, photons from left to right.

We plot $\Delta\phi$ for $H \rightarrow \tau\bar{\tau}$ events and separate them by the number of constituents in the jet, see Figure 8. We can see that the peak at $\Delta\phi = 0$ for charged constituents comes from jets with $n = 1$. What particles are these? Looking at Figure 9, we see that the peak at $\Delta\phi = 0$ comes from $n = 1$ where the single particle is an electron, muon or charged pion. This comes from following τ decays:

$$\begin{aligned}\tau^- &\rightarrow \pi^- + \bar{\nu}_\tau \\ \tau^- &\rightarrow e^- + \bar{\nu}_e + \nu_\tau \\ \tau^- &\rightarrow \mu^- + \bar{\nu}_\mu + \nu_\tau\end{aligned}$$

If there is only one constituent, then the relative angle is not defined. We get $\Delta\phi = \arctan(\frac{0}{0})$ which is set to 0.

Now let's consider $n = 2$. We see two peaks at $\pm\frac{\pi}{2}$ for electrons and photons. We consider the process of $\tau^- \rightarrow e^- + \bar{\nu}_e + \nu_\tau \rightarrow e^- + \bar{\nu}_e + \nu_\tau + \gamma$ where the electron emits

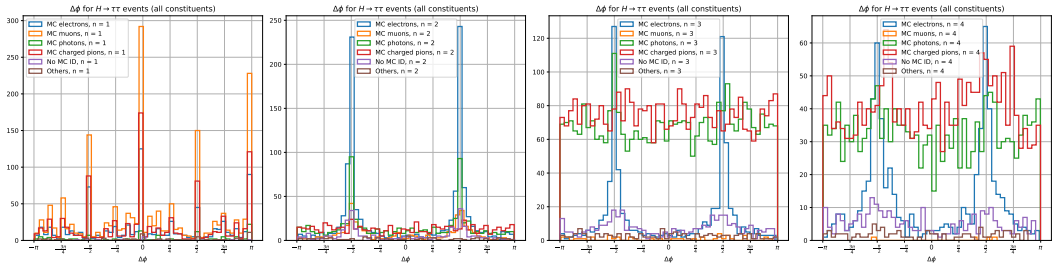


Figure 9: Separating the $\Delta\phi$ distribution by the MC particle ID for $H \rightarrow \tau\bar{\tau}$ events. Number of constituents per jet increases from one to four from left to right.

a Bremsstrahlung photon. In this case the photon and electron will have the same θ angle because the electron is only bend in the xy -plane due to the magnetic field along z . At the interaction point the ϕ angle will also be very similar. How is $\Delta\phi$ calculated? It is $\Delta\phi = \arctan \frac{p_y}{p_x}$ considering the momentum p after a rotation of the constituent around ϕ, θ of the jet. Because $\Delta\phi \in [-\pi, \pi]$ but $\arctan \in [-\frac{\pi}{2}, \frac{\pi}{2}]$ we need to consider the points $\pm \frac{\pi}{2}$ where tan goes to $\pm\infty$ depending on which side we are approaching. If p_x, p_y are very close to 0 but $p_x \ll p_y$ then we are approaching $\frac{\pi}{2}$. Depending on the signs we end up at $\pm \frac{\pi}{2}$. Why this is the case we be intuitively understood: Consider a jet as a cone. First, we rotate the cone on the x -axis and then flip it on the z -axis. The momentum of the jet will then point along the z -axis and has no component in x or y . Now consider a small plane that is spanned by a particle with the same θ and similar ϕ as the jet. After the rotation, the plane will be along the y axis due to the similar angle in ϕ and does not lay along x due to the same angle in θ . This is why $p_x \ll p_y$ is true for these events. The mathematical derivation can be found in Section 4.

This explains why Bremsstrahlung photons and the corresponding electrons have peaks at the $\Delta\phi$ distribution at $\pm \frac{\pi}{2}$.

The distributions rise a second question: Why do we see these smeared peaks around $\pm \frac{\pi}{2}$ for neutral particles as well? What is the physical explanation for similar θ and similar ϕ ? When we print these events, we see that the reconstruction often goes wrong. High energetic charged particle often get reconstructed as the charged particle plus an artificial neutron. This is then a fake neutron. As both, charged particle and neutron, are actually the same particle, the angles between them are very similar in the reconstruction. The high energetic charged particles are likely the leading particles in the jet, so that the jet momentum is highly dominated by them. We can then observe the same strange behavior for the relative angle as for Bremsphotons only that $\Delta\phi$ is more smeared out.

To wrap up this section: the observed distribution in $\Delta\phi$ arise from jet constituents with very similar angles to the jet. This can either be the case during the creation of Bremsstrahlung photons or due to fake neutrons belonging to a high energetic charged particle. One might consider the reconstruction algorithm to reduce the production of artificial neutrons.

4 Mathematical derivation of $\frac{\pi}{2}$ peaks

We calculate the relative angle in φ by rotating the momentum vector of the jet constituent by θ and φ of the jet. After the rotation the angle in φ is the relative angle between the jet constituent and the jet.

$$\vec{p}_{\text{rot}} = R_y(-\theta)R_z(-\varphi)\vec{p}$$

$$= \begin{pmatrix} \cos(-\theta) & 0 & \sin(-\theta) \\ 0 & 1 & 0 \\ -\sin(-\theta) & 0 & \cos(-\theta) \end{pmatrix} \begin{pmatrix} \cos(-\varphi) & -\sin(-\varphi) & 0 \\ \sin(-\varphi) & \cos(-\varphi) & 0 \\ 0 & 0 & 1 \end{pmatrix} \begin{pmatrix} p_x \\ p_y \\ p_z \end{pmatrix}$$

Using $\cos(-\theta) = \cos(\theta)$ and $\sin(-\theta) = -\sin(\theta)$,

$$\begin{aligned} &= \begin{pmatrix} \cos \theta & 0 & -\sin \theta \\ 0 & 1 & 0 \\ \sin \theta & 0 & \cos \theta \end{pmatrix} \begin{pmatrix} \cos \varphi & \sin \varphi & 0 \\ -\sin \varphi & \cos \varphi & 0 \\ 0 & 0 & 1 \end{pmatrix} \begin{pmatrix} p_x \\ p_y \\ p_z \end{pmatrix} \\ &= \begin{pmatrix} \cos \theta & 0 & -\sin \theta \\ 0 & 1 & 0 \\ \sin \theta & 0 & \cos \theta \end{pmatrix} \begin{pmatrix} \cos \varphi p_x + \sin \varphi p_y \\ -\sin \varphi p_x + \cos \varphi p_y \\ p_z \end{pmatrix} \\ &= \begin{pmatrix} \cos \theta(\cos \varphi p_x + \sin \varphi p_y) - \sin \theta p_z \\ -\sin \varphi p_x + \cos \varphi p_y \\ \sin \theta(\cos \varphi p_x + \sin \varphi p_y) + \cos \theta p_z \end{pmatrix} \end{aligned}$$

Through the momentum vector we can calculate the now relative angle to the jet in φ . The index j refers to the angle of the jet and the index c refers to the constituent. We substitute the momentum vector by the correlations to θ_c and φ_c :

$$\begin{aligned} \varphi_{\text{rel}} &= \arctan \left(\frac{p_{\text{rot},y}}{p_{\text{rot},x}} \right) \\ &= \arctan \left(\frac{-\sin \varphi p_x + \cos \varphi p_y}{\cos \theta(\cos \varphi p_x + \sin \varphi p_y) - \sin \theta p_z} \right) \end{aligned}$$

Using

$$p_x = p \sin \theta \cos \varphi_c, \quad p_y = p \sin \theta \sin \varphi_c, \quad p_z = p \cos \theta$$

$$= \arctan \left(\frac{-\sin(\varphi_j)p_c \sin(\theta_c) \cos(\varphi_c) + \cos(\varphi_j)p_c \sin(\theta_c) \sin(\varphi_c)}{\cos(\theta_j)(\cos(\varphi_j)p_c \sin(\theta_c) \cos(\varphi_c) + \sin(\varphi_j)p_c \sin(\theta_c) \sin(\varphi_c)) - \sin(\theta_j)p_c \cdot \cos(\theta_c)} \right)$$

We now consider photons from Bremsstrahlung so that $\theta_j = \theta_c = \theta$ because the electric field is in z direction.

$$\begin{aligned} &= \arctan \left(\frac{-\sin \varphi_j \sin \theta \cos \varphi_c + \cos \varphi_j \sin \theta \sin \varphi_c}{\cos \theta(\cos \varphi_j \sin \theta \cos \varphi_c + \sin \varphi_j \sin \theta \sin \varphi_c) - \sin \theta \cos \theta} \right) \\ &= \arctan \left(\frac{\sin \varphi_c \cos \varphi_j - \cos \varphi_c \sin \varphi_j}{\cos \theta(\cos \varphi_c \cos \varphi_j + \sin \varphi_c \sin \varphi_j) - \cos \theta} \right) \end{aligned}$$

Using $\sin(x-y) = \sin x \cos y - \cos x \sin y$ and $\cos(x-y) = \cos x \cos y + \sin x \sin y$ simplifies the expression:

$$= \arctan \left(\frac{\sin(\varphi_c - \varphi_j)}{\cos \theta(\cos(\varphi_c - \varphi_j) - 1)} \right)$$

Let's assume $\varphi_c = \varphi_j + \epsilon$

$$= \arctan \left(\frac{\sin(\epsilon)}{\cos \theta(\cos(\epsilon) - 1)} \right)$$

What is the limit as $\epsilon \rightarrow 0$?

Looking at the argument of arctan and using Taylor expansions we get:

$$\begin{aligned}
\frac{\sin(\epsilon)}{\cos(\epsilon) - 1} &\approx \frac{\epsilon - \frac{\epsilon^3}{3!} + \frac{\epsilon^5}{5!} + \mathcal{O}(\epsilon^7)}{1 - \frac{\epsilon^2}{2!} + \frac{\epsilon^4}{4!} - \frac{\epsilon^6}{6!} + \mathcal{O}(\epsilon^8) - 1} \\
&= \frac{1 - \frac{\epsilon^2}{3!} + \frac{\epsilon^4}{5!}}{\frac{\epsilon}{2!} + \frac{\epsilon^3}{4!} - \frac{\epsilon^5}{6!}} \\
&= \underbrace{\frac{1}{\frac{\epsilon}{2!} + \frac{\epsilon^3}{4!} - \frac{\epsilon^5}{6!}}} - \underbrace{\frac{\frac{\epsilon^2}{3!}}{\frac{1}{2!} + \frac{\epsilon^2}{4!} - \frac{\epsilon^4}{6!}}} + \underbrace{\frac{\frac{\epsilon^4}{5!}}{\frac{1}{2!} + \frac{\epsilon^2}{4!} - \frac{\epsilon^4}{6!}}} \quad \xrightarrow{\epsilon \rightarrow 0} -\infty \\
&= \underbrace{\frac{1}{0} = \infty}_{\text{for } \epsilon \rightarrow 0} \quad \underbrace{\frac{0}{-\frac{1}{2!+0}} = 0}_{\text{for } \epsilon \rightarrow 0} \quad \text{as for all other higher order terms}
\end{aligned}$$

We can conclude that

$$\lim_{\epsilon \rightarrow 0} \arctan \left(\frac{\sin(\epsilon)}{\cos \theta(\cos(\epsilon) - 1)} \right) = \arctan(-\infty) = -\frac{\pi}{2}$$

If $\varphi_c = \varphi_j - \epsilon$, we get the opposite sign for the limit:

$$\lim_{\epsilon \rightarrow 0} \arctan \left(\frac{-\sin(\epsilon)}{\cos \theta(\cos(\epsilon) - 1)} \right) = +\frac{\pi}{2}$$

5 Conclusion

We compared the observables describing jets and their constituents extracted from full and fast simulation for the H to bb channel. The distributions look similar. In the future, we might want to consider correcting some of the parameters due to the shift of the interaction point to the primary vertex. By comparing the H to $q\bar{q}$ ($q \in u, d, c, s, b$) and H to $\tau\bar{\tau}$ channels in full simulation with each other, we can conclude correctness for these channels too. We observe fake neutrons belonging to high energetic charged particles studying these distributions.

References

- [1] numpy.histogram. <https://numpy.org/doc/stable/reference/generated/numpy.histogram.html#numpy.histogram>. Accessed: 2024-06-17.
- [2] BEDESCHI, F., GOUSKOS, L., AND SELVAGGI, M. Jet flavour tagging for future colliders with fast simulation. *The European Physical Journal C* 82, 7 (July 2022).

Appendix

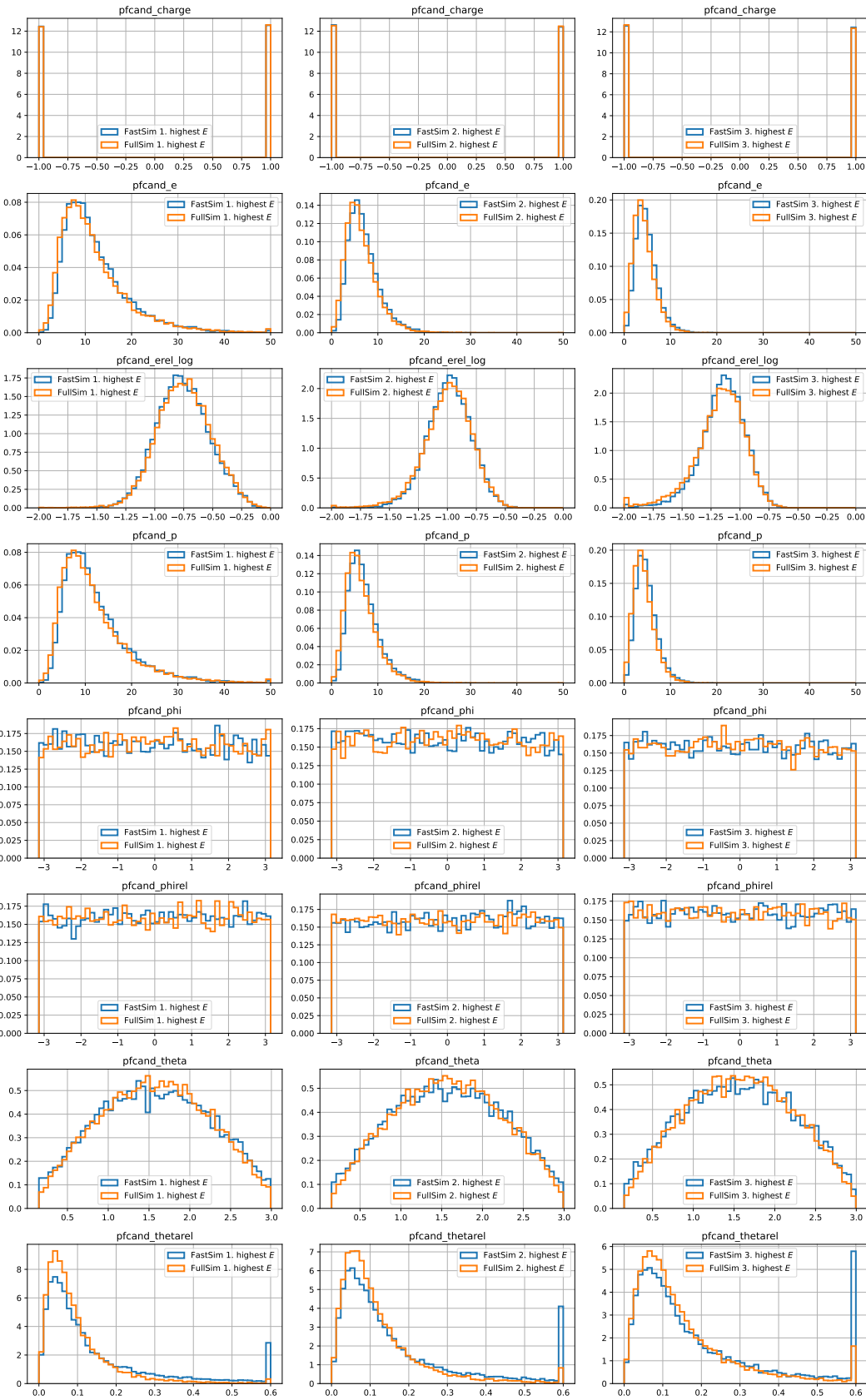


Figure 10: Properties of the three leading (leading, subleading, third from left to right) charged particles in fast (blue) and full (orange) simulation

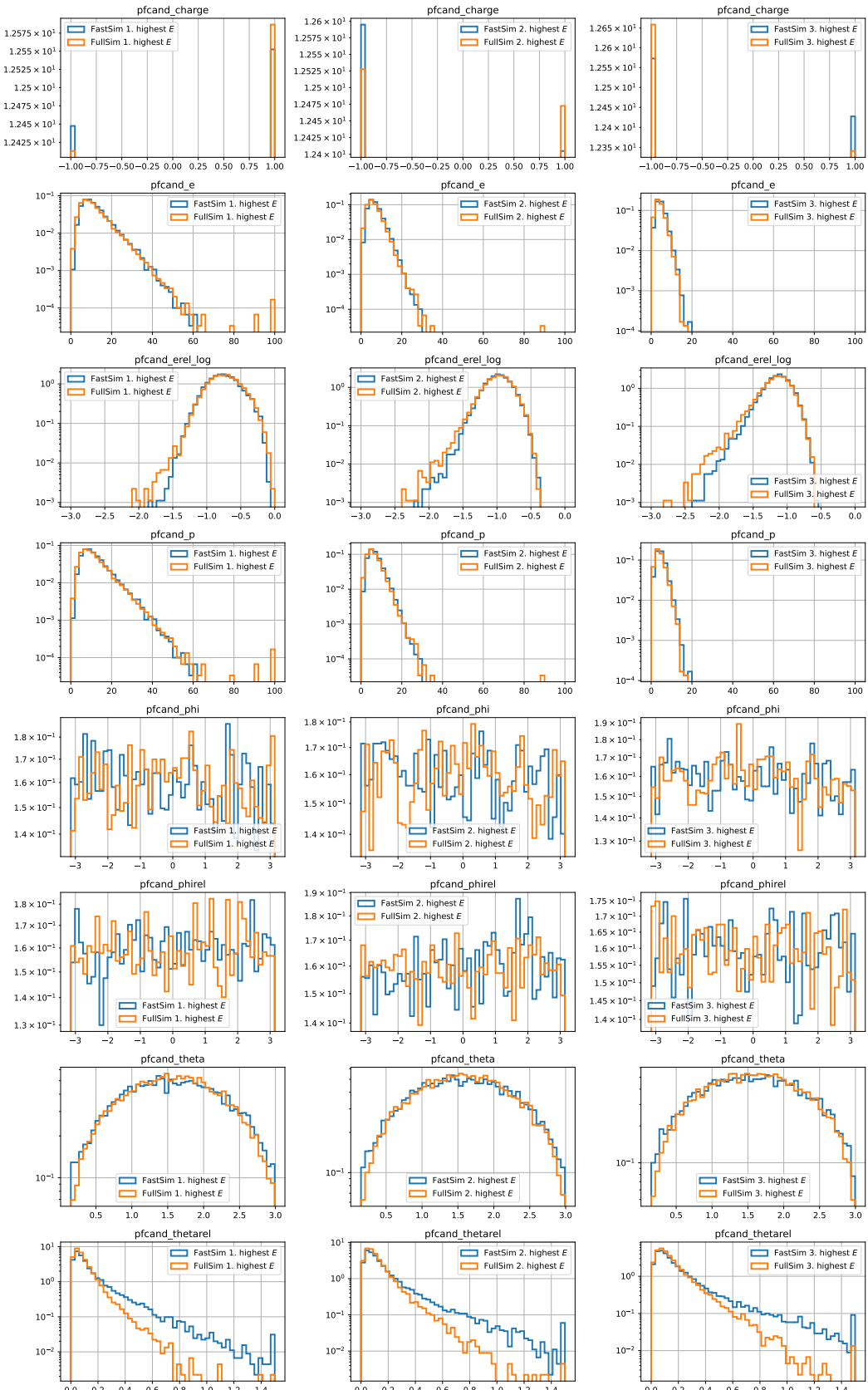


Figure 11: Properties of the three leading charged particles in fast (blue) and full (orange) simulation in logarithmic scale

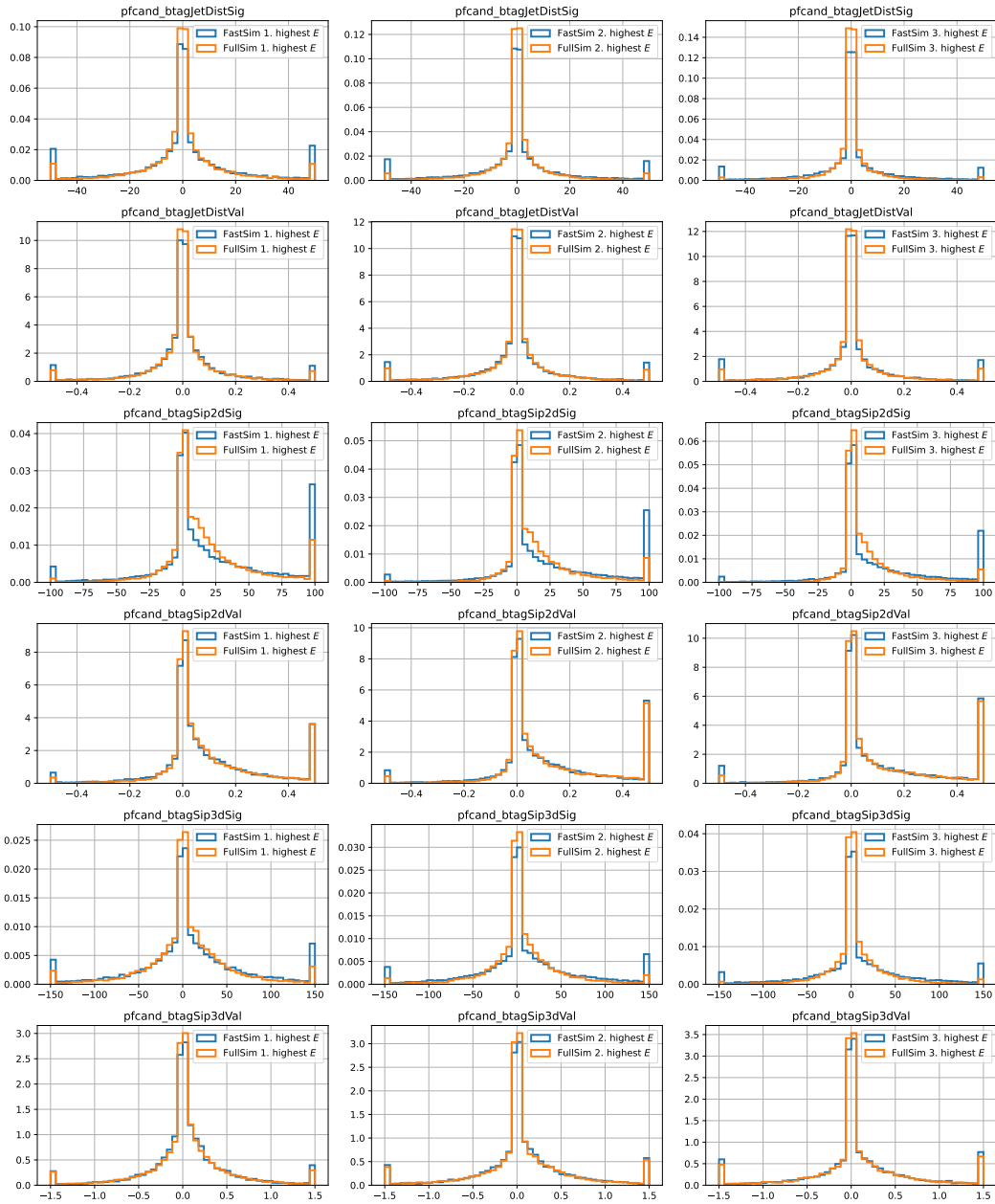


Figure 12: SIP and distance to point of closest approach of the three leading (leading, sub-leading, third from left to right) charged particles in fast (blue) and full (orange) simulation

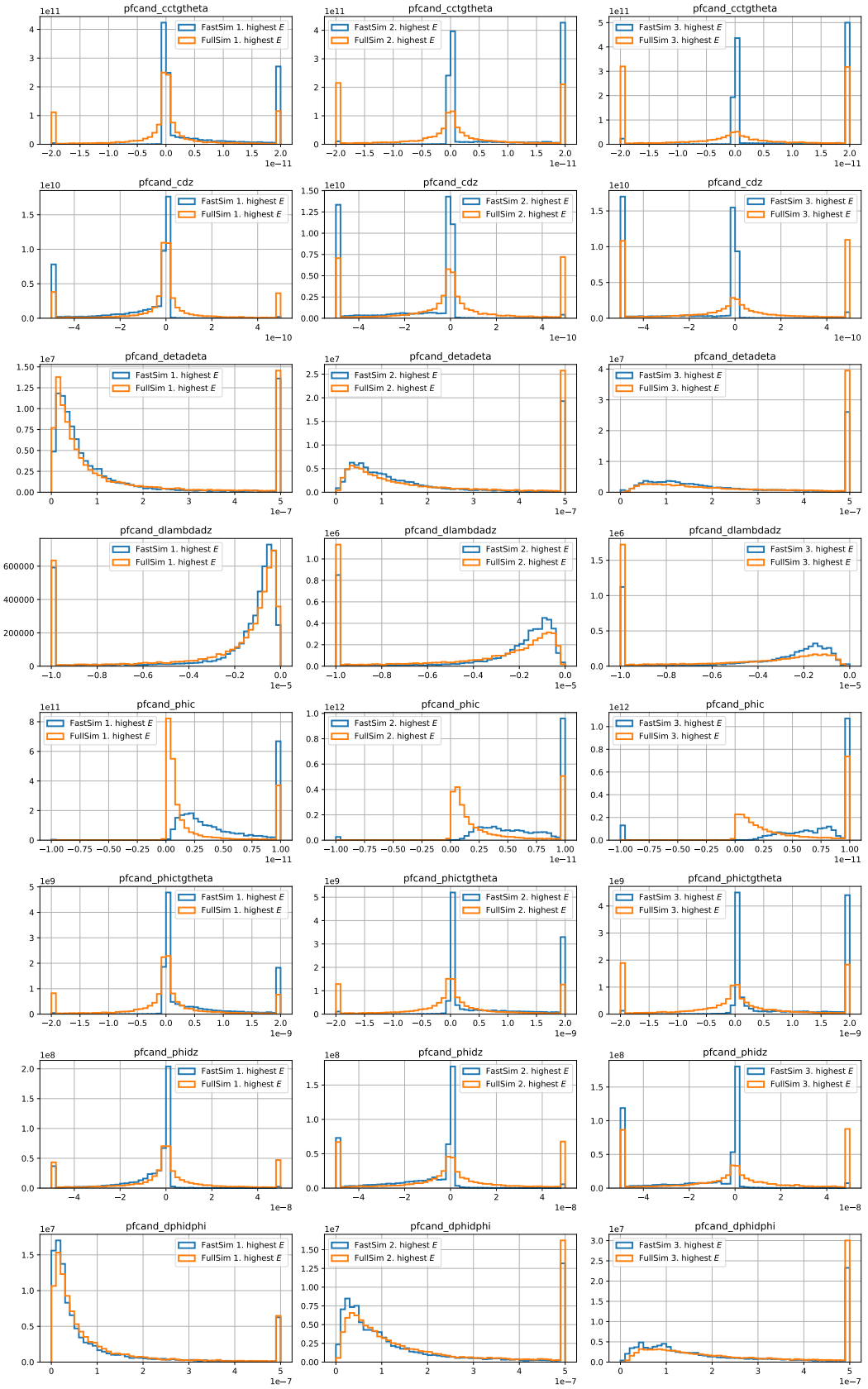


Figure 13: Covariance matrix for charged particles in fast (blue) and full (orange) simulation

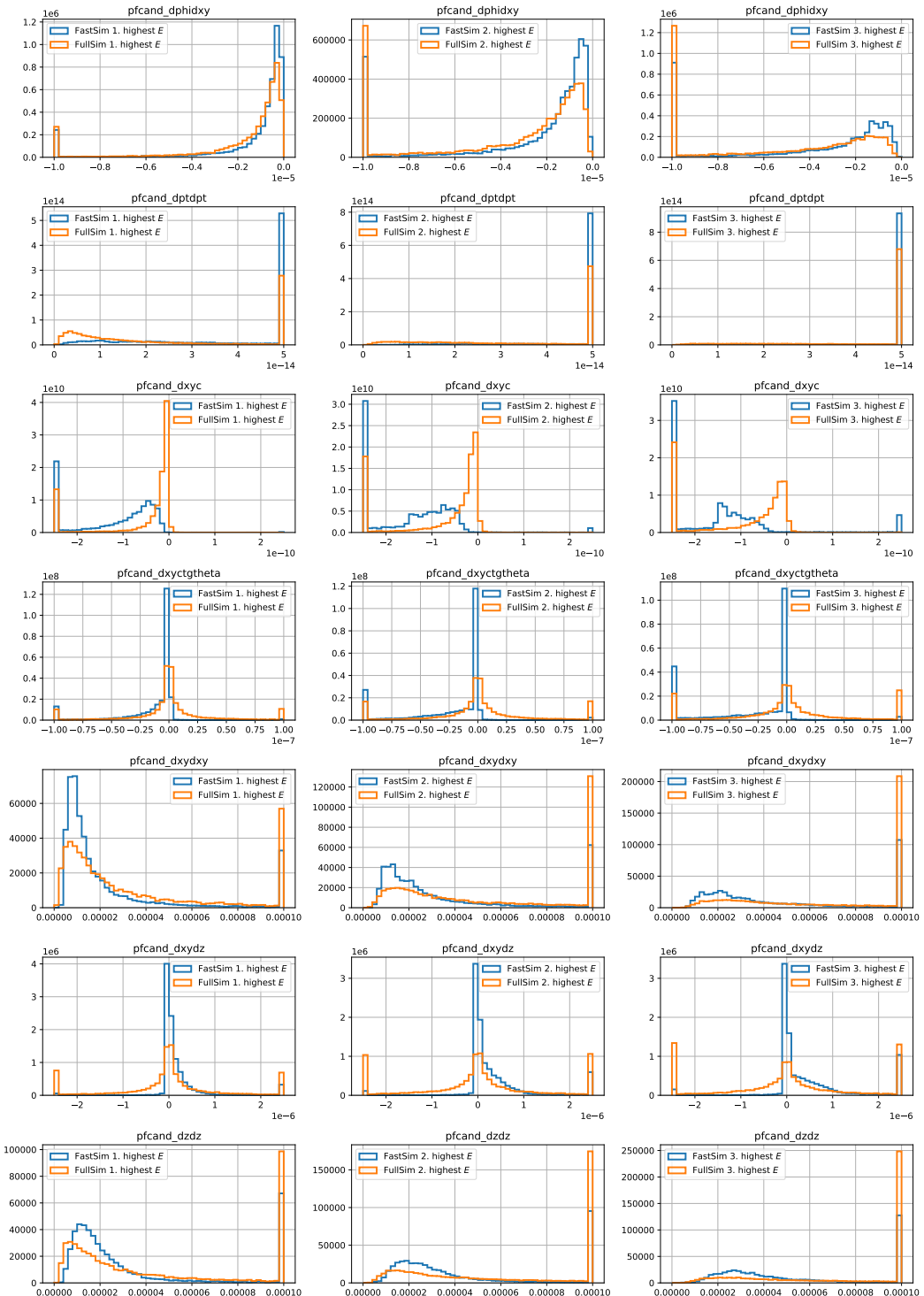


Figure 14: Covariance matrix for charged particles in fast (blue) and full (orange) simulation

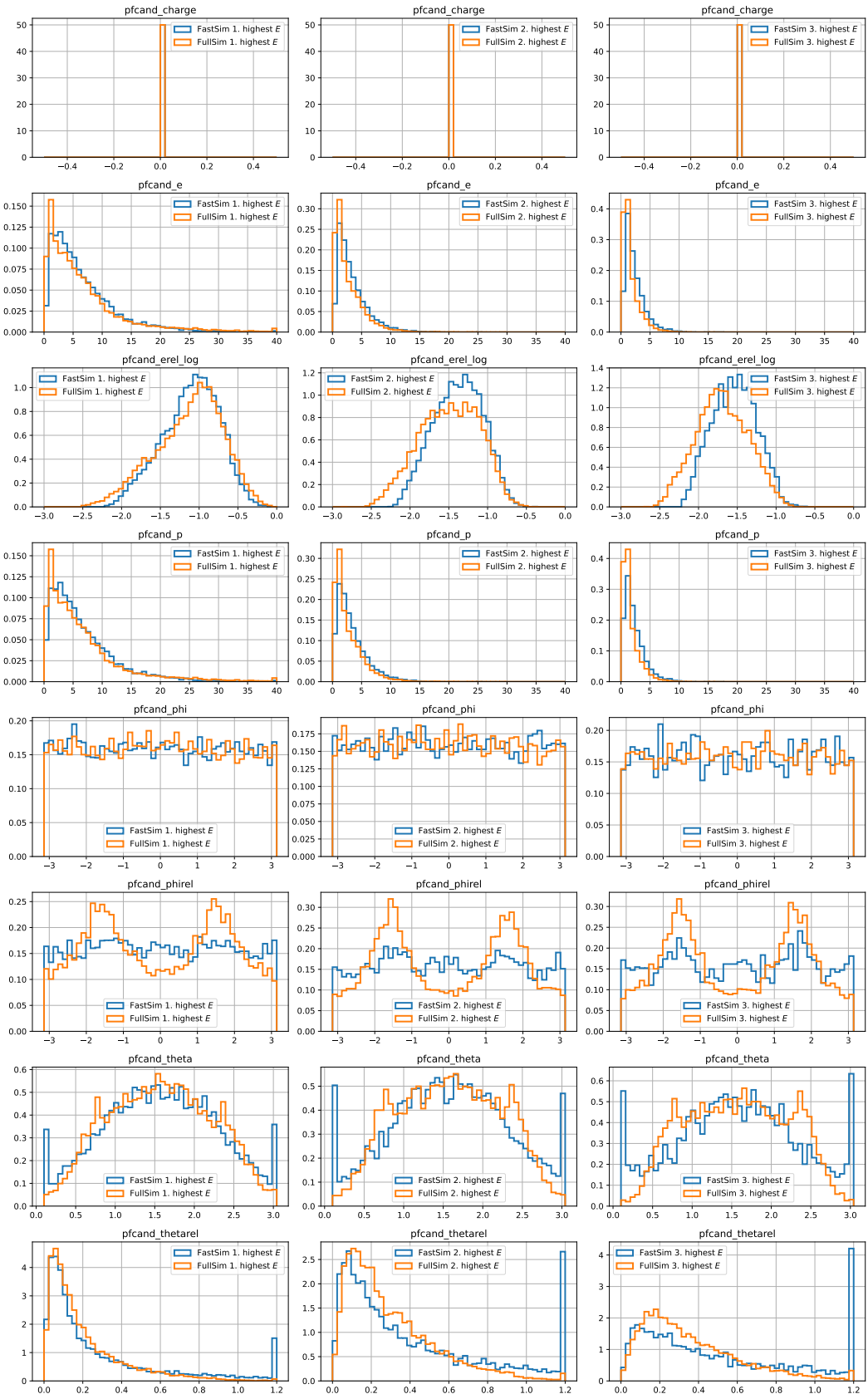


Figure 15: Properties of the three leading (leading, subleading, third from left to right) neutral hadrons in fast (blue) and full (orange) simulation

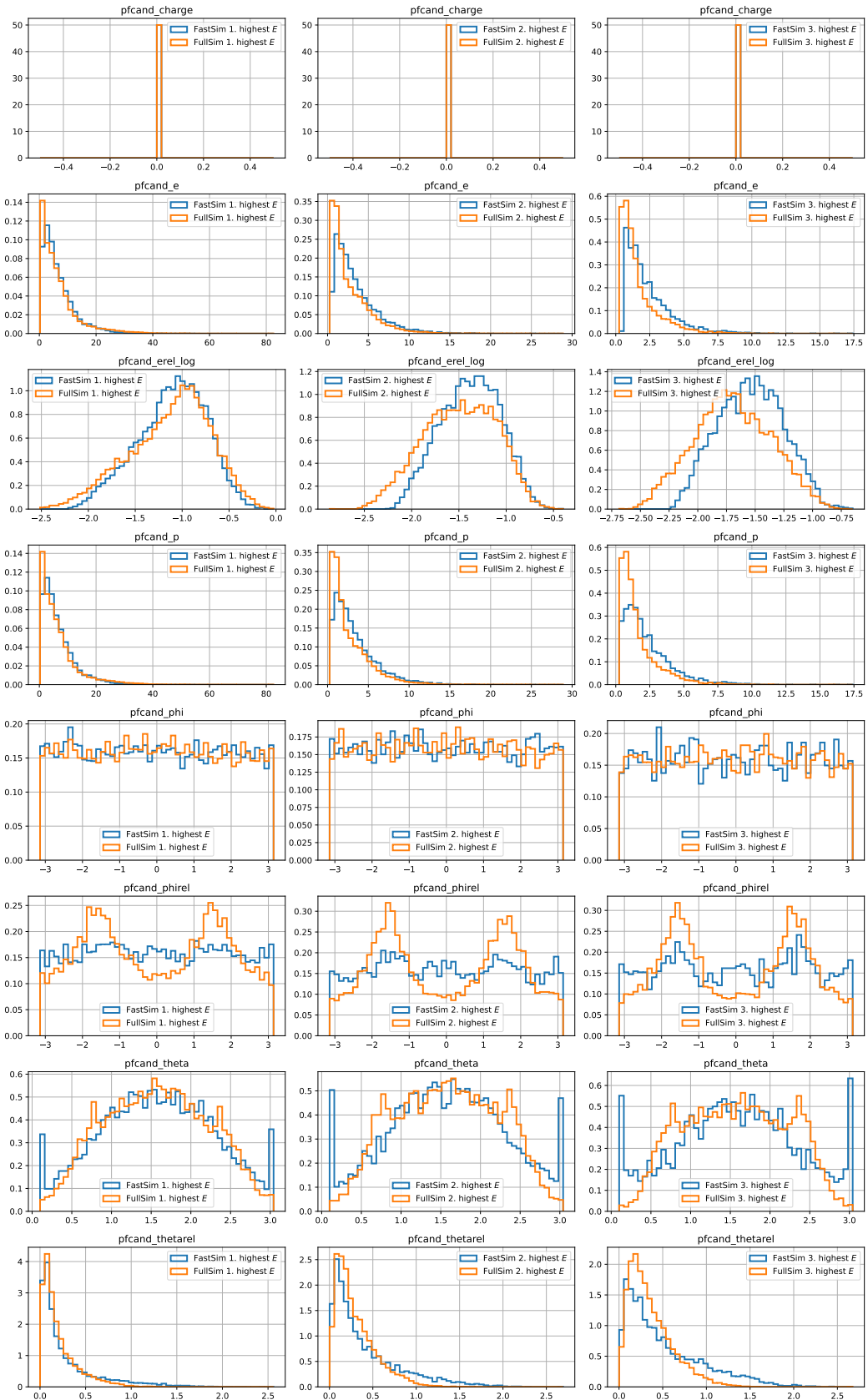


Figure 16: Properties of the three leading (leading, subleading, third from left to right) photons in fast (blue) and full (orange) simulation

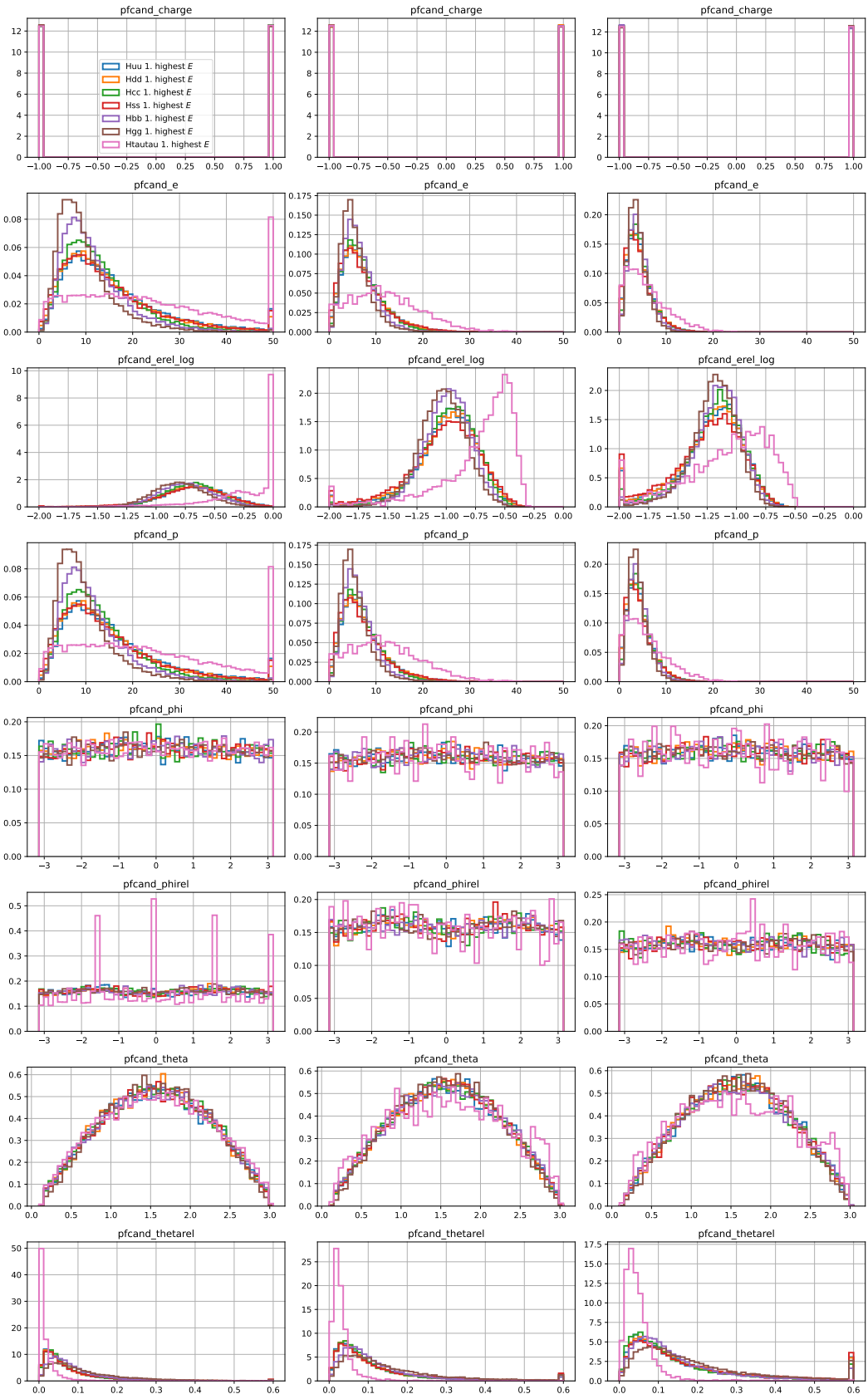


Figure 17: Properties of the three leading (leading, subleading, third from left to right) charged particles for different Higgs channels₁₉

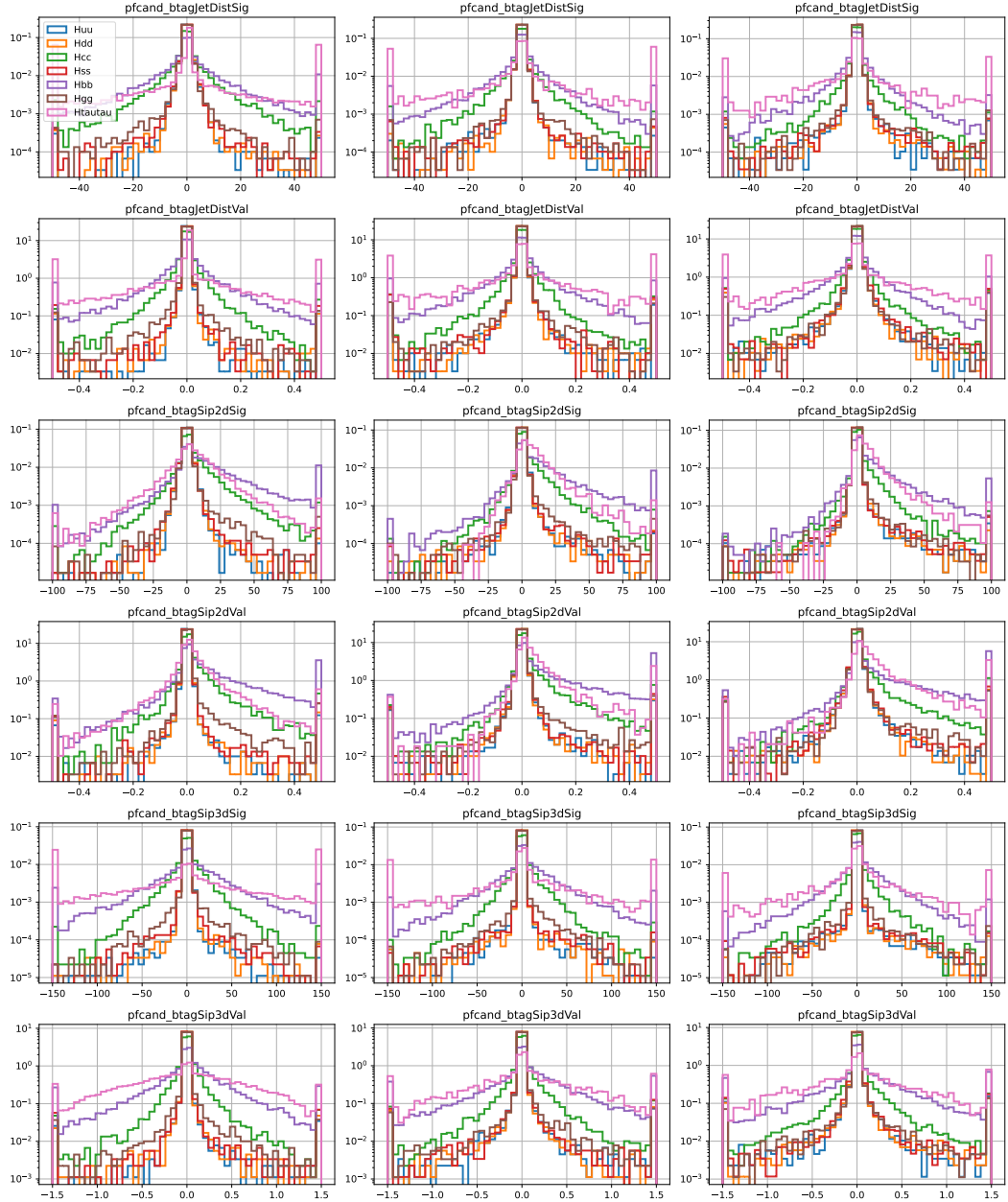


Figure 18: SIP and distance to point of closest approach of the three leading (leading, subleading, third from left to right) charged particles for different Higgs decay channels in full simulation

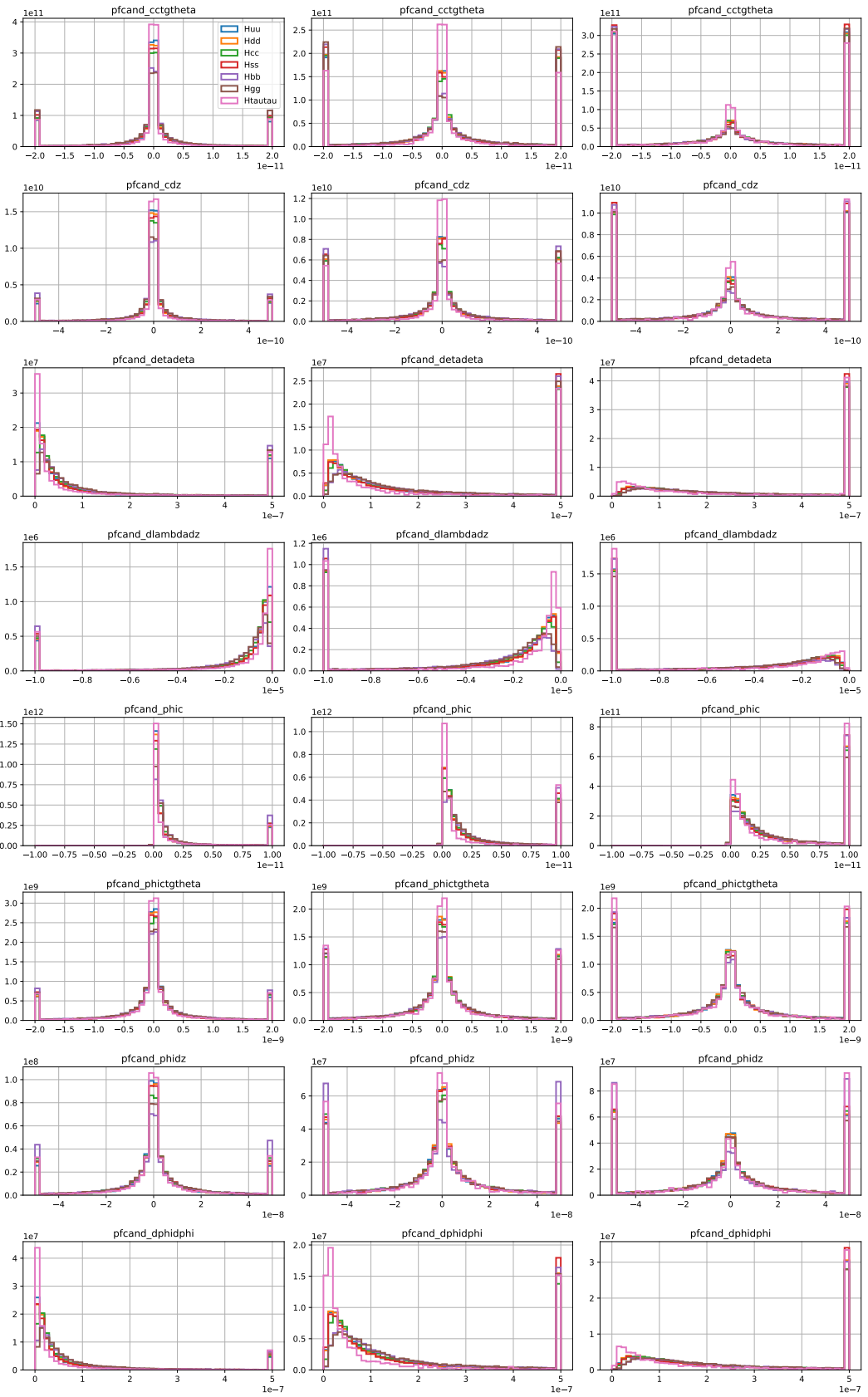


Figure 19: Covariance matrix for charged particles (leading, subleading, third from left to right) for different Higgs decay channels in full simulation

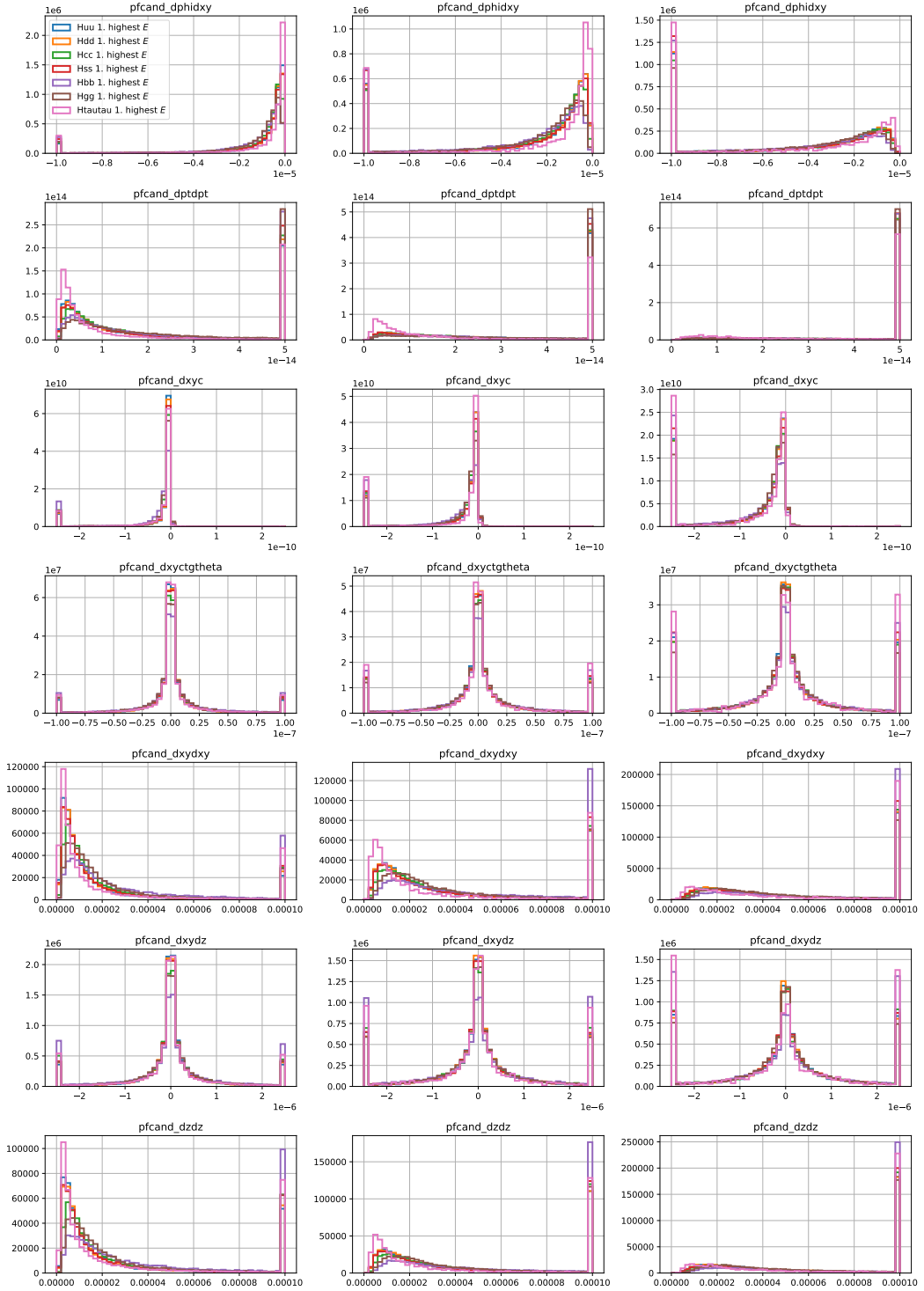


Figure 20: Covariance matrix for charged particles for different Higgs decay channels in full simulation

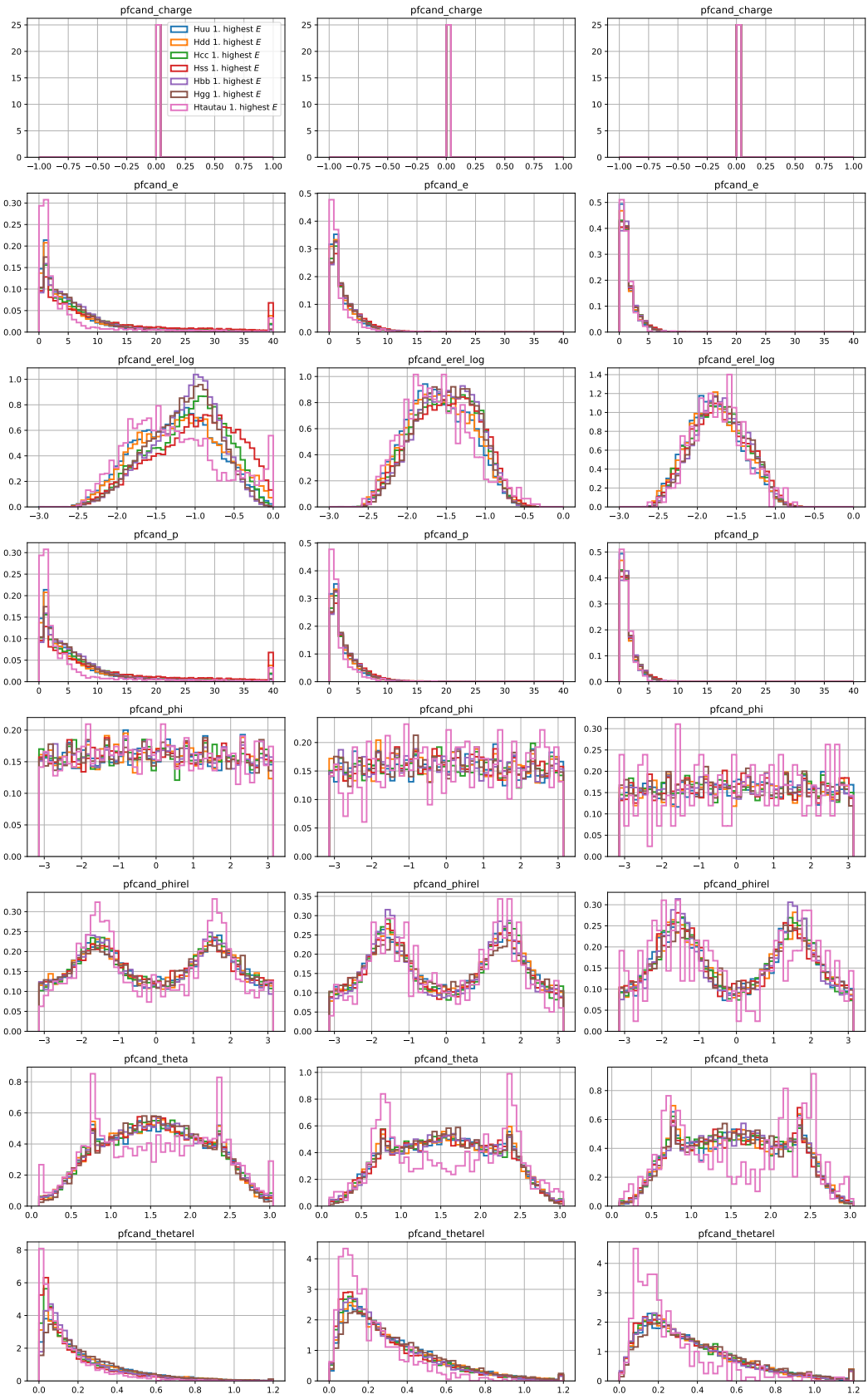


Figure 21: Properties of the three leading (leading, subleading, third from left to right) neutral hadrons for different Higgs decay channels in full simulation

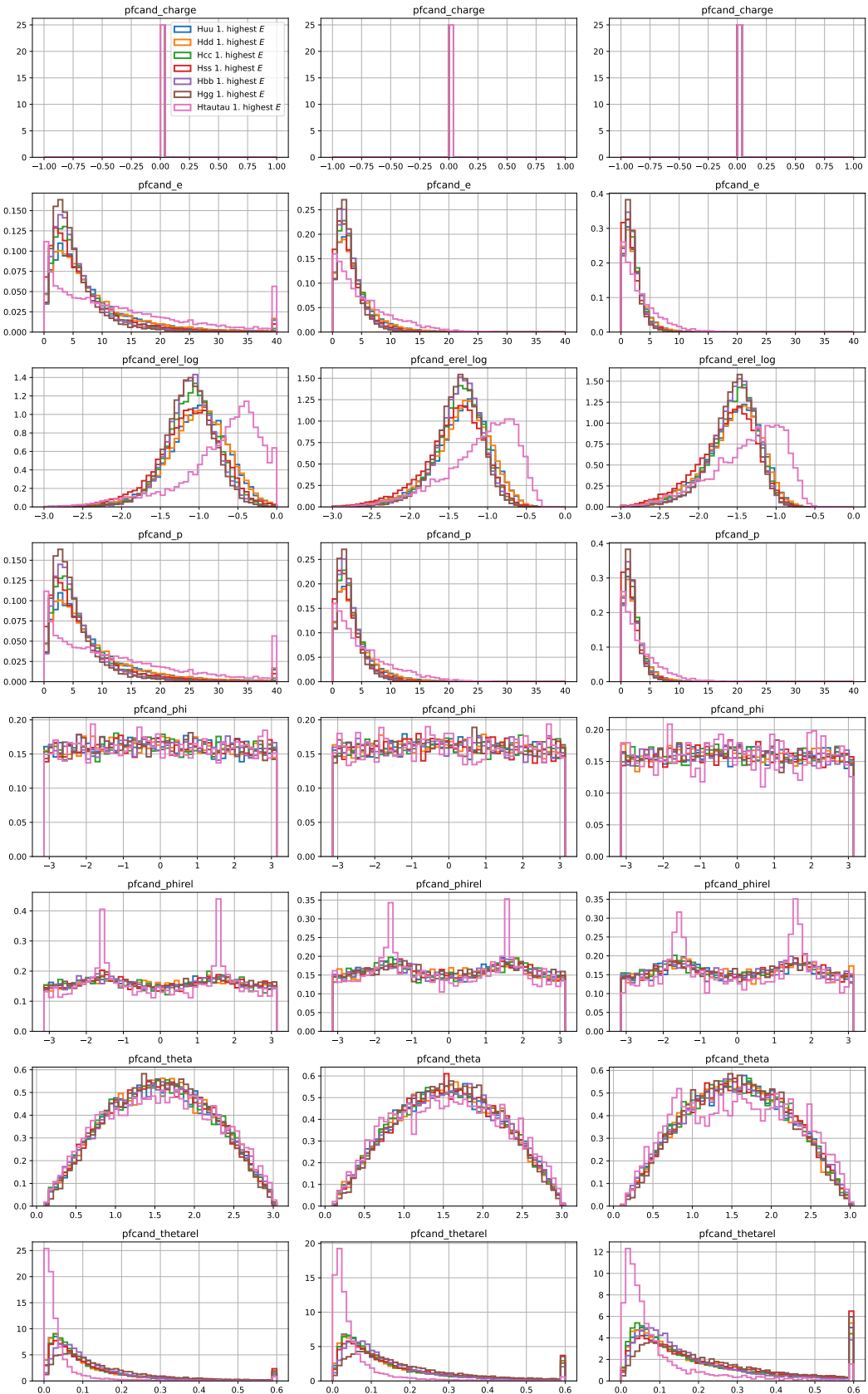


Figure 22: Properties of the three leading (leading, subleading, third from left to right) photons for different Higgs decay channels in full simulation